

Double - Diffusive Convection in Molten Pb - Sn Alloy

M. T. Hyun* · T. L. Bergman**

용융상태인 납 - 주석 합금의 이중확산유동

현 명 택 · T. L. Bergman

Key words : Double - diffusive convection(이중확산유동), Chebyshev collocation technique (체비셰프 콜로케이션 기법), Finite volume method(유한체적법), Buoyancy ratio (부력비)

Abstract

액체 상태인 Pb - Sn 합금에 의한 이중확산유동에 대해 체비셰프 콜로케이션 기법을 이용하여 수치해석하였다. 온도차에 의한 부력과 농도차에 의한 부력이 작을 때에는 유동형태가 서서히 준정상상태에 이르러 아무런 진동현상을 볼 수 없다. 부력이 증가함에 따라 유동은 수직 농도 경계층을 파괴하여 플룸(Plume) 형태의 유동을 생성시키고, 이는 시스템 내부로 성장한 후 소멸된다. 이러한 현상이 반복되면서 높은 주파수의 진동현상을 관찰할 수 있다.

Nomenclature

C : dimensionless concentration = $(C' - C_1)/(C_h - C_1)$	L : half length or height of the enclosure, m
C_h : concentration of high concentration wall, wt%	N : buoyancy ratio = $\beta_C \cdot (C_h - C_l) / \beta_T \cdot (T_h - T_c)$
C_l : concentration of low concentration wall, wt%	p : pressure, N/m ²
D : mass diffusivity, m ² /s	Pr : Prandtl number = ν/α
g : gravitational acceleration, m/s ²	Ra : Rayleigh number = $g\beta_T(T_h - T_c)(2L)^3/(\nu \cdot \alpha)$
Gr_S : solutal Grashof number = $Ra \cdot N/Pr$	Sc : Schmidt number = ν/D
	Sh : local Sherwood number = $\partial C(t, -1, y)/\partial x$
	\bar{Sh} : mean Sherwood number = $\int_{-1}^1 (\partial C(t, -1, y)/\partial x) dy$

* 정회원, 제주대학교

** Department of Mechanical Engineering, The University of Texas at Austin, Austin, TX 78712

- T : dimensionless temperature = $(T' - T_c)/(T_h - T_c)$
 T_c : temperature of cold wall, $^{\circ}\text{C}$
 T_h : temperature of hot wall, $^{\circ}\text{C}$
 t : dimensionless time = $t' \nu/L^2$
 u : dimensionless x - direction velocity = $u'L/\nu$
 v : dimensionless y - direction velocity = $v'L/\nu$
 x : dimensionless horizontal coordinate = x'/L
 y : dimensionless vertical coordinate = y'/L
 α : thermal diffusivity, m^2/s
 β_C : coefficient of solutal expansion = $1/\rho(\partial\rho/\partial C)_{T,p}$
 β_T : coefficient of thermal expansion = $-1/\rho(\partial\rho/\partial T)_{C,p}$
 ν : kinematic viscosity, m^2/s
 ρ : density, kg/m^3
 Ψ : dimensionless stream function = Ψ'/ν
 ω : dimensionless vorticity = $\omega'L^2/\nu$

Subscripts

- crit : critical
i : initial
max : maximum value
min : minimum value

Superscript

- : dimensional value

1. Introduction

Double - diffusive convection occurs in low Pr liquids during solidification of metals and semiconductor materials. It is well known that convection plays a major role in determining the species and crystalline distribution in the final product and, in turn, product properties. Simulation is motivated primarily by experimental difficulties involving low Pr liquids and, in the

main, finite volume methods¹⁾ have been used to predict the solidification process²⁻⁵⁾.

Although simulations have revealed interesting behavior, it is unclear whether the liquid phase transport is accurately predicted. Indeed, the extremely fine three dimensional structure and oscillatory behavior which has been observed experimentally in cavity convection involving moderate Pr, high Sc liquids^{6,7)} suggests that accurate simulation of thermosolutal convection at high Gr_S is extremely difficult, if not impossible. In this study, liquid phase convection in molten Pb - Sn is simulated using a Chebyshev collocation(spectral) method. New double - diffusive phenomena is revealed at high Gr_S with the direct simulation, and the predicted onset of oscillatory behavior is consistent with theory based upon experimental observation.

2. Mathematical Model

The system considered is two dimensional convection of Pb - Sn in a square enclosure of dimension $2L$. The cavity top and bottom are insulated, while the left and right faces are held at uniform cold and hot temperature, respectively. All cavity walls are impermeable, but the left and right faces are maintained at Sn - rich(light) and Pb - rich(heavy) uniform concentrations. Hence, thermal(solutal) buoyancy forces induce counter clockwise(clockwise) circulation. Note that i) opposing thermosolutal liquid phase buoyancy forces are established during solidification of Pb - rich, Pb - Sn alloys and ii) fine three dimensional structure may be embedded within the overall two dimensional flow⁶⁾.

Preliminary studies showed that vorticity - velocity formulation of the convective behavior resulted in a faster numerical algorithm rela-

tive to stream function – vorticity or primitive variable formulations. Nearly identical predictions were generated with the different formulations, and the simulations reported here approximately 6 months CPU time on an IBM RS/6000 350 workstation. The governing equations in terms of vorticity – velocity functions are (with the origin at the cavity center) :

$$\partial^2 v / \partial x^2 + \partial^2 v / \partial y^2 = \partial \omega / \partial x \quad (1)$$

$$\partial^2 u / \partial x^2 + \partial^2 u / \partial y^2 = - \partial \omega / \partial y \quad (2)$$

$$\begin{aligned} 8 \cdot \text{Pr} \cdot ((\partial \omega / \partial t + u \cdot \partial \omega / \partial x + v \cdot \partial \omega / \partial y) \\ - (\partial^2 \omega / \partial x^2 + \partial^2 \omega / \partial y^2)) \\ = \text{Ra} \cdot (\partial T / \partial x - N \cdot \partial C / \partial x) \end{aligned} \quad (3)$$

$$\begin{aligned} \text{Pr} \cdot (\partial T / \partial t + u \cdot \partial T / \partial x + v \cdot \partial T / \partial y) \\ = \partial^2 T / \partial x^2 + \partial^2 T / \partial y^2 \end{aligned} \quad (4)$$

$$\begin{aligned} \text{Sc} \cdot (\partial C / \partial t + u \cdot \partial C / \partial x + v \cdot \partial C / \partial y) \\ = \partial^2 C / \partial x^2 + \partial^2 C / \partial y^2 \end{aligned} \quad (5)$$

The boundary and initial conditions are :

$$\begin{aligned} u(t, \pm 1, y) = u(t, x, \pm 1) = v(t, \pm 1, y) \\ = v(t, x, \pm 1) = 0 \end{aligned} \quad (6a)$$

$$\begin{aligned} T(t, -1, y) = 0, T(t, 1, y) \\ = 1, \partial T(t, x, \pm 1) / \partial y = 0 \end{aligned} \quad (6b)$$

$$\begin{aligned} C(t, -1, y) = 1, C(t, 1, y) \\ = 0, \partial C(t, x, \pm 1) / \partial y = 0 \end{aligned} \quad (6c)$$

$$\begin{aligned} u(0, x, y) = v(0, x, y) = 0, T(0, x, y) \\ = 0.5x + 0.5, C(0, x, y) = 0.5 \end{aligned} \quad (6d)$$

Equations (1) – (5) were solved using a Chebyshev collocation technique⁹. In short, the dependent variable spatial distributions are expanded in doubly truncated series of Chebyshev polynomials using the usual Chebyshev – Gauss – Lobatto quadrature points⁹. Time integration is achieved by a finite difference technique using the AB/second order backward Euler procedure, which combines implicit treatment of the diffusion terms (to improve numerical stability) with explicit treatment of the advection terms (to avoid iteration). This procedure, when applied to Eqs.(3) – (5), results in a two dimensional

Helmholtz equation at each time level. A full matrix diagonalization algorithm⁹ is used to solve the Helmholtz and Poisson Eqs.(1) and (2). Computational details are discussed in Madabhushi et al.¹⁰ and Hyun et al.¹¹ and are not repeated here.

As shown by Hyun et al.¹¹, the predictions are insensitive to the time step (10^{-5} to 10^{-6}) and spatial resolution (65×65 to 177×177 spatial modes) with a rapid and accelerating rate of convergence (of the L^2 – norm for the concentration field at a given time, as well as for the time – averaged \bar{Sh} history) with spatial resolution. In addition, predictions have been compared to those of the finite volume method, and at $\text{Ra} = 5000$, $N = -10$ the two techniques produce highly disparate result¹². The large discrepancy is attributed to numerical diffusion in the finite volume method which, in turn, dampens high frequency fluctuation.

3. Results

Simulations were performed for a lead – rich, Pb – Sn mixture. Although there is uncertainty regarding the thermophysical properties of this alloy⁵, they were taken to be $\text{Pr} = 0.02$ and $\text{Sc} = 150$. Note that 8 and 18 equally spaced contours are drawn for the positive stream function and concentration distributions in Figs. 1 – 4, while negative stream function values are listed in the figure captions. Since they are not interesting, temperature distributions are not shown.

Selected concentration and stream function distributions for $\text{Ra} = 100$, $N = -10$ are shown in Fig. 1. Under conditions of low thermal buoyancy, the system response consists of Pb – (Sn –) rich liquid falling (rising) along the right (left) cavity face with solutally – stratified conditions eventually existing throughout the enclosure

(Fig. 1d). Thermal buoyancy forces induce counter clockwise core rotation and, with time the core shrinks due to interaction with the clockwise rotation associated with solutal buoyancy forces.

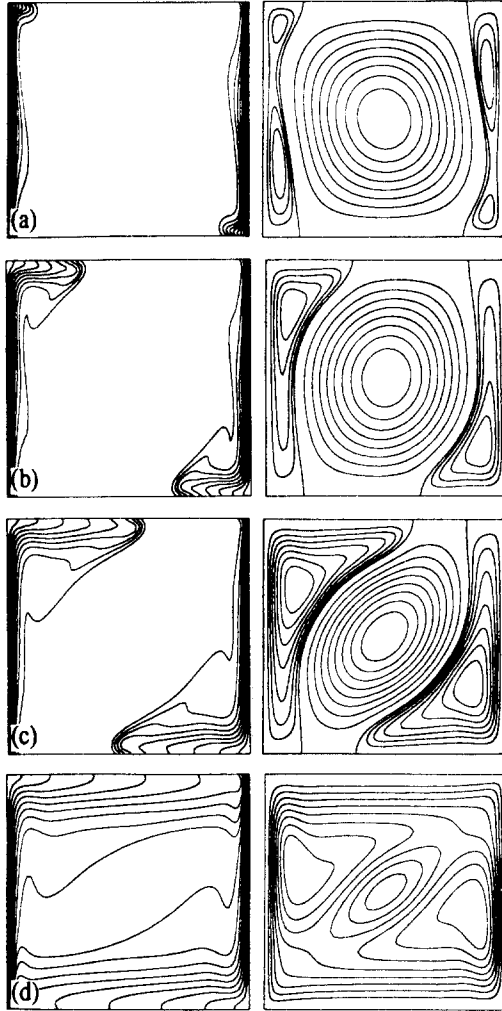


Fig. 1 Predicted concentration and stream function distributions for $Ra=100$ and $N=-10$ at (a) $t=0.3$ ($\psi_{max}=4.94$, $\psi_{min}=-0.189$, $\psi=-0.047, -0.095, -0.142$), (b) $t=0.75$ ($\psi_{max}=3.895$, $\psi_{min}=-0.385$, $\psi=-0.077, -0.154, -0.231, -0.308$), (c) $t=1.35$ ($\psi_{max}=1.883$, $\psi_{min}=-0.466$, $\psi=-0.058, -0.117, 0.175, -0.233, -0.291, -0.350, -0.408$), (d) $t=3.15$ ($\psi_{max}=0.321$, $\psi_{min}=0$).

Relative to the response at low buoyancy, conditions for $Ra=5000$, $N=-10$ (Fig. 2) show fundamentally different behavior. The concentration distributions are complicated by a thermally-affected entrainment process along the edge of the species boundary layers at, approxi-

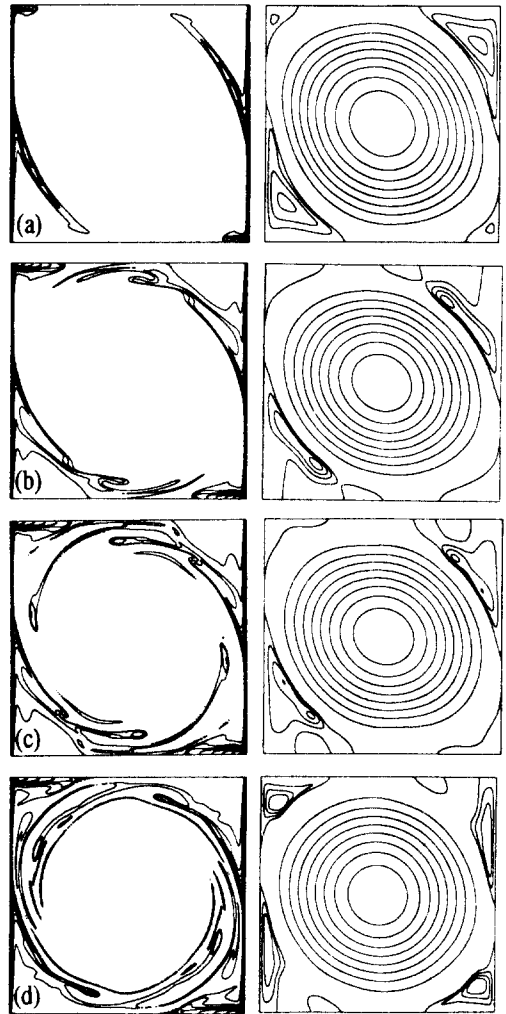


Fig. 2 Predicted concentration and stream function distributions for $Ra=5000$ and $N=-10$ at (a) $t=0.06$ ($\psi_{max}=124.3$, $\psi_{min}=-0.97$, $\psi=0.3, 0.6, 0.9$), (b) $t=0.14$ ($\psi_{max}=141.7$, $\psi_{min}=-2.1$, $\psi=-0.6, -1.2, -1.8$), (c) $t=0.17$ ($\psi_{max}=144.7$, $\psi_{min}=-1.6$, $\psi=-0.5, 1.0, -1.5$), (d) $t=0.22$ ($\psi_{max}=152.2$, $\psi_{min}=-0.89$, $\psi=-0.2, -0.4, -0.6$).

mately, cavity mid - height(Fig. 2a). Rather than being smoothly incorporated into the core, the entrained liquid is broken into small drops which are subsequently advected thermally throughout the domain. Breakup times are random and, as will be shown, the intermittent nature of the flow leads to a high frequency temporal variation in the Sh history. Droplet trajectory dominated by its solutal buoyancy force component, as observed experimentally by Jiang et al.⁶, was not noted here. A much less robust, yet intermittent entrainment phenomena was found at $Ra = 1000$, $N = -10$ (Ref. 11). Simulation of the $Ra = 5000$, $N = -10$ case using the finite volume method produced no high frequency behavior or solutal boundary layer breakup by Hyun et al.¹².

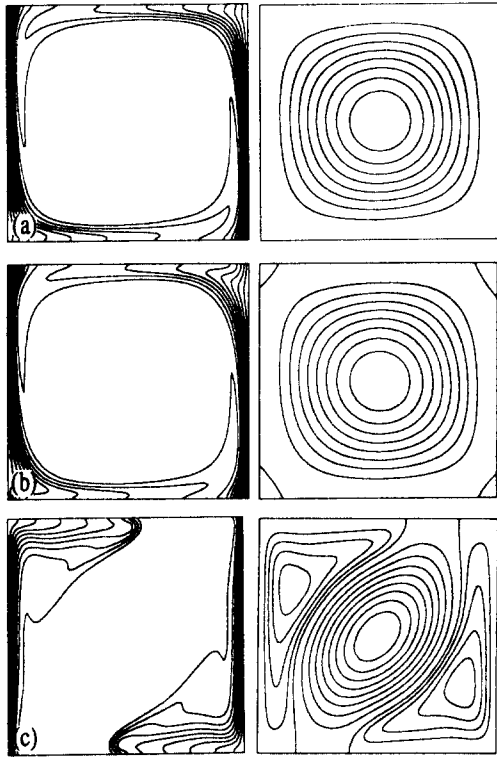


Fig. 3 Predicted concentration and stream function distributions for $Ra = 100$ and $t = 1.35$: (a) $N = 0.1$ ($\psi_{max} = 6.305$, $\psi_{min} = 0$), (b) $N = -1$ ($\psi_{max} = 6.20$, $\psi_{min} = -0.003$), (c) $N = -10$ ($\psi_{max} = 1.883$, $\psi_{min} = -0.466$, $\psi = 0.1, -0.2, -0.3, -0.4$).

Figures 3 and 4 include predicted behavior at particular times for $Ra = 100$ (Fig. 3) and 5000 (Fig. 4) under a range of solutal buoyancy conditions. At either Ra value, increasing N from -0.1 to -1 modestly affects the system response. Only slight variation in the concentration distribution is noted, along with the establishment of corner recirculations at $N = -1$. As N is increased further to -10 (Figs. 3c and 4c), however, transition to overall downflow(upflow) along the right(left) wall is noted along with advancing solutal fronts at the cavity ceiling and floor in Fig. 3c, while a complex species distribution is evident in Fig. 4c.

Local Sh distributions are reported in Fig. 5

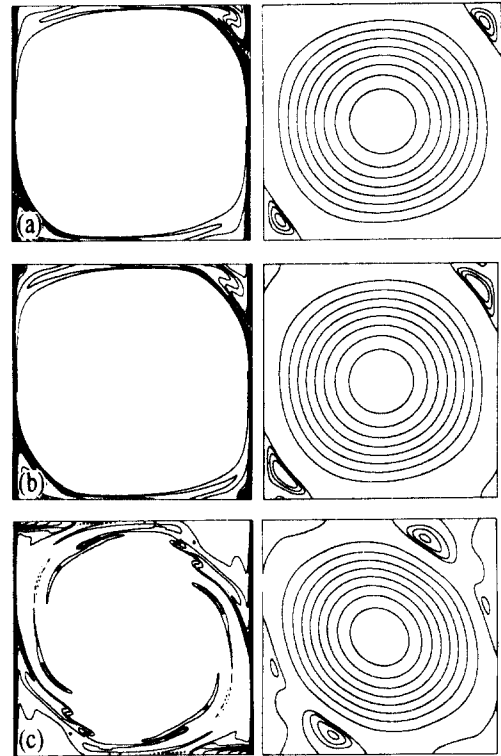


Fig. 4 Predicted concentration and stream function distributions for $Ra = 5000$ and $t = 0.18$: (a) $N = -0.1$ ($\psi_{max} = 170.0$, $\psi_{min} = -0.249$, $\psi = -0.07, -0.14, -0.21$), (b) $N = -1$ ($\psi_{max} = 170.0$, $\psi_{min} = -0.440$, $\psi = -0.1, -0.2, -0.3$), (c) $N = -10$ ($\psi_{max} = 146.2$, $\psi_{min} = -3.260$, $\psi = -1.0, -2.0, -3.0$).

for the $Ra=100$ and 5000 results of Figs. 3 and 4(Figs. 5a and 5b, respectively). At low Ra , significant solutal buoyancy forces($N=-10$) trigger a severe redistribution in local species transport rates in response to the wall flow reversal noted in Fig. 3c. Local Sh minima are evident in Fig. 5b, and coincide with wall flow stagnation regions most notably evident in Fig. 4c. Note that i) wall stagnation regions have been observed experimentally^{6,7)} and ii) the Sh distribution is not smooth at $Ra=5000$, $N=-10$ because of the intermittent breakup of the solutal boundary layer.

Because of the tenacity with which liquids retain their solutal identity(high Sc), interpretation of the boundary layer breakup and entrainment process is difficult if $0 \leq C \leq 1$ is plotted. Figure 6 includes a series of concentration contours for $0 \leq C \leq 0.45$ (Pb - rich liquid).

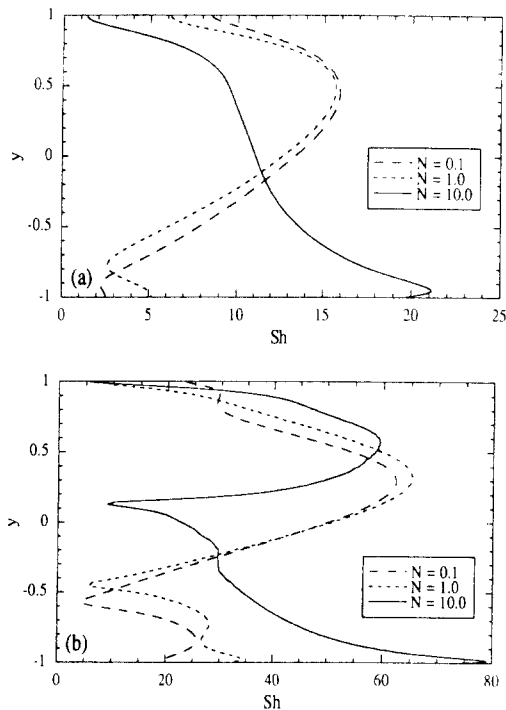


Fig. 5 Local Sh with buoyancy ratio along left wall : (a) $Ra=100$ and $t=1.35$, (b) $Ra=5000$ and $t=0.18$.

Close inspection shows that i) droplet formation dynamics are extremely complex, and are different for separate droplets(compare drops 2 and 4), ii) droplet formation is affected by proximity to the cavity ceiling(drop 3), iii) the droplet life span varies(compare drops 1 and 2), iv) the droplet shape is affected by vorticity(drop 1, Figs. 6f, g and h) and v) the frequency of drop formation is very high compared to the rate at which the Pb - rich fluid falls along the right wall to the cavity floor. The influence of the drop longevity(drops of Pb - rich liquid are injected into cold fluid regions, resulting in significant local subcooling relative to the material's liquidus) on potential solidification dynamics is quantified in Hyun et al.¹²⁾.

Selected Sh histories are shown in Fig. 7. Since $C_i=0.5$, Sh is initially infinite and predictions are insensitive to buoyancy forces until convective motion is established. In each case, predicted histories are similar for $N=-0.1$ and -1 , with major variations associated with $N=-10$. At $Ra=1000$ (Fig. 7b) Sh is reduced at $N=-10$ due to i) the establishment of a solutally - inactive core region and ii) absence of significant high frequency mixing as shown in Hyun et al.¹¹⁾. In contrast, Sh is enhanced at $N=-10$ for $Ra=100$ (Fig. 7a) and $Ra=5000$ (Fig. 7c) by i) overall flow reversal and the "filling box" behavior at small Ra and ii) establishment of high frequency mixing at large Ra .

To further examine the high frequency behavior, Fig. 7d shows part of the Sh histories for i) $Ra=5000$, $N=-10$ and ii) $Ra=2500$, $N=-20$. These extreme, $Gr_S^{1/4} \approx 40$ predictions are in the experimental range of Jiang et al.⁷⁾, and the values of N bracket N_{crit} which marks the transition between their fluctuating and quasi-steady experimental results. Consistent with the experimentation, the $Ra=5000$ case is characterized by high frequency fluctuation,

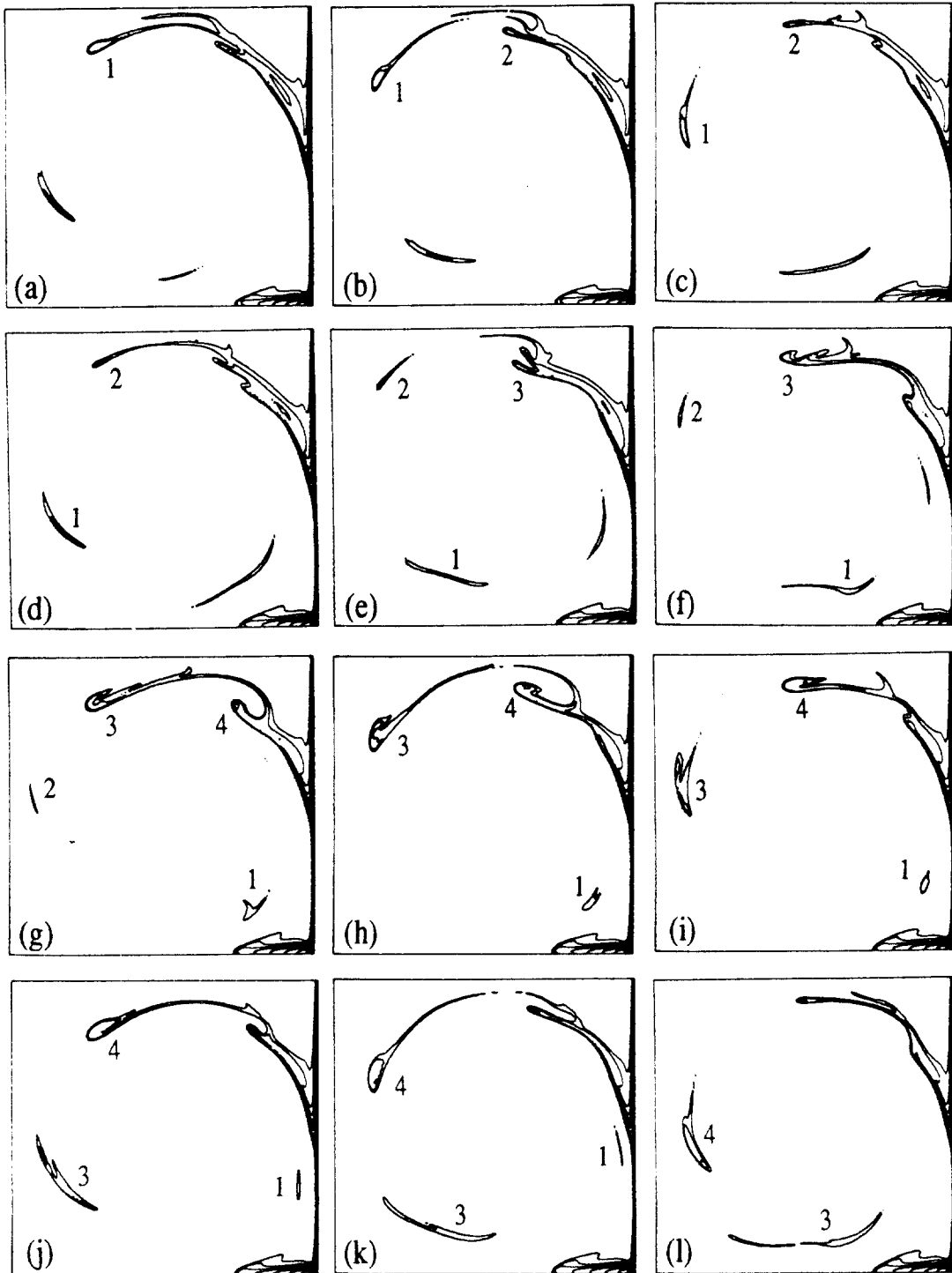


Fig. 6 Time series of Pb rich concentration contours. The initial is $t=0.175$ and results are shown at time increments of 0.0025. Contour values are shown for $0 \leq C \leq 0.45$ in increments of 0.05. Individual drops are identified.

while the $Ra=2500$ case experiences only modest, low frequency variation with time. Considering that i) the experiments were performed with a moderate Pr liquid in shallow enclosures, and ii) the observed flow was character-

ized by fine three dimensional structure, it is remarkable that present two dimensional simulations exhibit transition to high frequency, thermosolutally - driven oscillatory behavior in a manner with the experimentally - based theory.

4. Summary and Conclusions

In this study, a spectral method was used to predict two dimensional double - diffusive convection in a low Pr liquid. Under some conditions, a highly complex yet realistic concentration distribution is induced by thermal convection which triggers high frequency system response related to the breakdown of the solutal boundary layer. The transition from quasi - steady to high frequency oscillatory convection is consistent with the criterion developed by Jinang et al.⁷. Since finite volume method simulations produced no transition, and since most solidification simulations employ the finite volume method, it is probable that some solidification simulations do not adequately predict relevant liquid phase convection.

Features which might be addressed include the effects of three - dimensionality and response in other aspect ratio enclosures. Solidification dynamics may be included, although the details concerning their inclusion in a direct simulation are unclear at this time. Experimental validation of the predicted complex concentration distributions in a low Pr melt is desirable.

Acknowledgement

The first author would like to thank the Korea Science and Engineering Foundation for financial assistance.

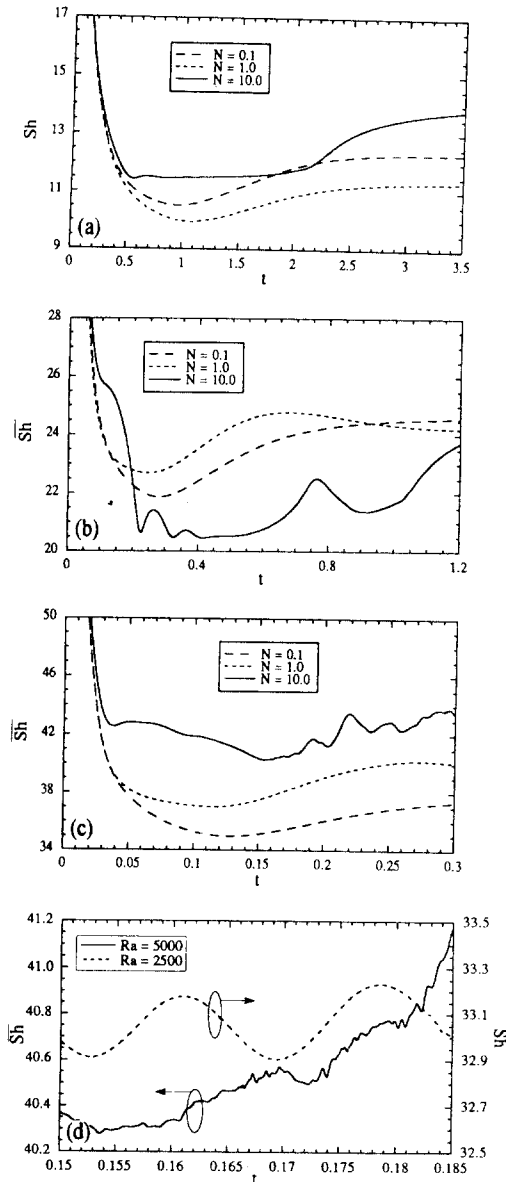


Fig. 7 Predicted Sh histories with buoyancy ratio : (a) $Ra=100$, (b) $Ra=1000$, (c) $Ra=5000$, (d) detailed histories for $Ra=5000$ and 2500 .

References

- 1) S.V. Patankar, Numerical Heat Transfer and Fluid Flow, McGraw - Hill, New York, 1980.
- 2) D. Xu and Q. Li, "Numerical Method for Solution of Strongly Coupled Binary Alloy Solidification Problems," Numerical Heat Transfer A, Vol. 20, pp. 181 - 201, 1991.
- 3) P.J. Prescott and F.P. Incropera, "Numerical Simulation of a Solidifying Pb - Sn Alloy : The Effects of Cooling Rate on Thermosolutal Convection and Macrosegregation," Metallurgical Transactions B, Vol. 22B, pp. 529 - 540, 1991.
- 4) H. Shahani, G. Amberg and H. Fredriksson, "On the Formation of Macroseggregations in Unidirectionally Solidified Sn - Pb and Pb - Sn Alloys," Metallurgical Transactions A, Vol. 23A, pp. 2301 - 2311, 1992.
- 5) P.J. Prescott and F.P. Incropera, "Convective Transport Phenomena and Macrosegregation During Solidification of a Binary Metal Alloy - I. Numerical Predictions," Journal of Heat Transfer, Vol. 116, pp. 735 - 741, 1994.
- 6) H.D. Jiang, S. Ostrach and Y. Kamotani, "Thermosolutal Convection Flow Regimes with Opposed Buoyance Forces in Shallow Enclosures," PCH PhysicoChemical Hydrodynamics, Vol. 10, pp. 599 - 613, 1988.
- 7) H.D. Jiang, S. Ostrach and Y. Kamotani, "Unsteady Thermosolutal Transfer Phenomena Due to Opposed Buoyance Forces in Shallow Enclosures," Journal of Heat Transfer, Vol. 113, pp. 135 - 140, 1991.
- 8) U. Ehrenstein and R. Peyret, "A Chebyshev Collocation Method for the Navier - Stokes Equations with Application to Double - Diffusive Convection," International Journal for Numerical Methods in Fluids, Vol. 9, pp. 427 - 452, 1989.
- 9) C. Canuto, M.Y. Hussaini, A. Quarteroni and T.A. Zang, Spectral Methods in Fluid Dynamics, Springer, New York, 1988.
- 10) R.K. Madabhushi, S. Balachandar and S.P. Vanka, "A Divergence - Free Chebyshev Collocation Procedure for Incompressible Flows with Two Non - Periodic Direction," Journal of Computational Physics, Vol. 105, pp. 199 - 206, 1993.
- 11) M.T. Hyun, D.C. Kuo, T.L. Bergman and K.S. Ball, "Direct Simulation of Double Diffusion in Low Pr Liquids," Numerical Heat Transfer, 1995(in press).
- 12) M.T. Hyun, D.C. Kuo, T.L. Bergman and K.S. Ball, "Simulation of Thermosolutal Convection in Pb - Sn : FVM and Spectral Predictions," Proceedings of the 1995 National Heat Transfer Conference, 1995(in press).